

# Electromagnetic Engineering of a Single-Mode Nanolaser on a Metal Plasmonic Strip Placed into a Circular Quantum Wire

Olga V. Shapoval, *Member, IEEE*, Kazuya Kobayashi, *Senior Member, IEEE*, and Alexander I. Nosich, *Fellow, IEEE*

**Abstract**—We investigate the emission of waves by a thin silver nanostrip placed into the center of a circular quantum wire (QWR), in the visible-light range. Our analysis uses the mathematically grounded approach called lasing eigenvalue problem (LEP). Keeping in mind that at the threshold the lasing-mode frequency is real valued (does not attenuate in time), the LEP is formulated as a boundary-value problem for the Maxwell equations with exact boundary conditions and the Sommerfeld radiation condition. The eigenvalues are pairs of real numbers, where the first is the emission wavelength and the second is the associated threshold value of material gain in the QWR. Due to the twofold symmetry of the cross-sectional geometry, we split the studied problem into four different independent classes of symmetry and derive four symmetry-adapted Green's functions of the QWR without strip. On imposing the generalized boundary conditions and taking into account these Green's functions, we obtain four independent integral equations (IEs) at strip's median line. We discretize these IEs with the Nystrom-type schemes and further look for the eigenvalues of each class separately with the aid of iterative search algorithm. Our analysis shows that such a plasmonic-strip-based nanolaser can emit visible light on the localized surface plasmon modes and also on the shell modes or QWR polariton modes perturbed by the strip. Single-mode operation is apparently possible provided that the QWR diameter is small, and hence, the first shell mode is blue-shifted.

**Index Terms**—Strip nanolaser, quantum wire, localized surface plasmon, lasing eigenvalue problem, integral equation, Nystrom-type discretization, threshold gain.

## I. INTRODUCTION

**T**ODAY plasmonics has become a field of very active research within optics and photonics. Along with the progressively emerging nanotechnology, it offers many new and exciting applications and hence attracts considerable attention.

Manuscript received February 1, 2017; revised May 22, 2017; accepted June 5, 2017. This work was partially supported by the research fellowship of the Canon Foundation in Europe and the Young Scientist Grant of the President of Ukraine (Ф 63/39-2016) to the first author. (*Corresponding author: Olga V. Shapoval.*)

O. V. Shapoval and A. I. Nosich are with the Laboratory of Micro and Nano Optics, Institute of Radio-Physics and Electronics, National Academy of Sciences of Ukraine, Kharkiv 61085, Ukraine (e-mail: olga.v.shapoval@gmail.com; anosich@yahoo.com).

K. Kobayashi is with the Department of Electrical, Electronic, and Communication Engineering, Chuo University, Tokyo 192-0393, Japan (e-mail: kazuya\_k@sea.plala.or.jp).

Color versions of one or more of the figures in this paper are available online at <http://ieeexplore.ieee.org>.

Digital Object Identifier 10.1109/JSTQE.2017.2718658

This is mainly because of remarkable opportunities of enhanced light-matter interaction in nanoscale metal configurations, combined with controlled precision of fabrication. The physical basis of this enhanced interaction is provided by the existence of LSP modes on metal particles and wires due to specific properties of metal's dielectric functions in the optical range. More recently, an interest in exploiting the LSP modes for lasing has appeared. This has led to experimental demonstration of the smallest plasmonic laser based on the colloidal gold nanospheres enveloped in dye-doped shells [1]. Several papers dealt with simulation of nanolasers based on the circular metal nanowires equipped with active shells [2]–[4]. By now the attention has focused on the lasing in periodic arrays of nanoparticles immersed into an active layer [5]–[8] or in the presence of quantum wires [9]. In this paper, we explore the modes of another type of nanolaser: a thin silver nanostrip placed into an active shell in the form of QWR with circular cross-section. Following [10], such a configuration can be also viewed as a QWR decorated with a silver plasmonic nanostrip resonator, to stabilize QWR against blinking. We attack this problem with advanced method based on the combined use of the Lasing Eigenvalue Problem, the generalized boundary condition to characterize the strip, and the mathematically grounded Nystrom-type discretization of the associated singular and hyper-singular IEs.

LEP is the eigenvalue (source-free) electromagnetic field problem specifically tailored to provide both the modal frequencies and the associated values of threshold material gain in the active region [4], [9] and [11]–[14]. This is because, in contrast to the conventional eigenvalue problem based on the Q-factor theory for a passive optical cavity, LEP fully takes into account the size, shape and location of the active region. Note that other LEP-like formulations exist, for instance, see [15]–[18]; some of them differ from our approach only by the choice, within a constant, of the material-gain parameter.

We suppose that the electromagnetic field depends on time as  $e^{-i\omega t}$  ( $\omega$  being the cyclic frequency) and omit this factor throughout the rest of the paper. Here,  $k = \omega/c = 2\pi/\lambda$  is the free-space wavenumber, while  $c$  and  $\lambda$  are the free-space light velocity and the wavelength, respectively. Considering plasmonic nanostrip-in-QWR nanolaser shown in Fig. 1, we assume that it consists of a silver strip of the width  $2d$  and the thickness  $h$  immersed in the center of a QWR of the radius  $a$ . Silver's refractive index is denoted as  $\nu_{Ag} = \varepsilon_{Ag}^{1/2}$  where  $\varepsilon_{Ag}(\lambda)$  is the complex dielectric permittivity function, while QWR (the

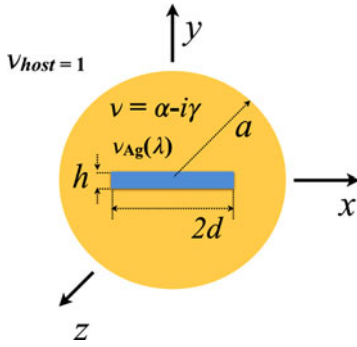


Fig. 1. Strip nanolaser cross-sectional geometry: Flat silver nanostrip placed into a circular QWR.

active region) has refractive index  $\nu = \alpha - i\gamma$ , where  $\alpha$  is a known positive value. In the lasing-mode analysis, we suppose that  $\gamma > 0$  is the unknown bulk material gain in QWR (under pump). For simplicity, we assume here that both  $\alpha$  and  $\gamma$ , do not depend on  $\lambda$ . As the lasing-mode frequency at threshold is real-valued, we follow [4] and [9], [11]–[14] and consider LEP in terms of finding the ordered pairs  $(\lambda, \gamma)_m$ , where  $\lambda_m > 0$  is the lasing-mode wavelength and  $\gamma_m$  is the associated threshold value of material gain in QWR ( $m$  stands for a generic mode index).

Note also that the gain per wavelength, frequently met in the description of lasers, is easily found as  $g = k\gamma$ . Still we do not use it here as we have found that it is convenient only in one-dimensional (1-D) case, which is for the Fabry-Perot or other flat-layered microcavities.

Some preliminary results of our analysis were published in contributed conference papers [19]–[21]. Here we present more details of the method used and fuller numerical data that enables us to draw important conclusions. The rest of the paper is organized as follows. In Section II, we formulate the LEP for the plasmon-assisted strip-in-QWR nanolaser and explain basic equations and mathematical details. In Section III, we present and discuss the numerical analysis of the lasing-mode spectrum of the considered nanolaser. Conclusions are summarized in Section IV. In Appendix, we present the analysis of auxiliary problem of the plane-wave scattering by a silver nanostrip placed into a circular dielectric rod.

## II. BASIC EQUATIONS

### A. LEP as an Electromagnetic Boundary-Value Problem

The function we are looking for is the  $H_z$  magnetic field component, which must satisfy the following boundary-value problem:

- 1) 2D Helmholtz equation off the boundaries.
- 2) Continuity conditions for the tangential field components on the circular contour of QWR.
- 3) Continuity conditions for the tangential field components at the strip contour.
- 4) Sommerfeld radiation condition at infinity.
- 5) Condition of the local power finiteness.
- 6) Two-fold symmetry conditions.

It is required to find the eigenvalues of such a non-traditional electromagnetic-field problem that are the ordered pairs of real numbers,  $(\lambda, \gamma)$  as explained above. Note that  $\lambda$  can be assumed real exactly because of the presence of threshold gain  $\gamma$  in the refractive index of the active region.

Real-life metal nanostrips have finite thickness. However if this thickness is a fraction of the free-space wavelength, then it can be neglected and the following two-side generalized boundary condition (GBC) can be imposed at the strip median line,  $S = (x, y) : x \in [-d, d], y = 0$ :

$$\partial[H_z^+(\vec{r}) + H_z^-(\vec{r})]/\partial\vec{n}(\vec{r}) = 2ikR[H_z^-(\vec{r}) - H_z^+(\vec{r})], \quad (1)$$

$$[H_z^+(\vec{r}) + H_z^-(\vec{r})] = 2iQ\partial[H_z^+(\vec{r}) - H_z^-(\vec{r})]/\partial\vec{n}(\vec{r}). \quad (2)$$

Here, the coefficients  $R$  and  $Q$  are the so-called relative electric and magnetic resistivities,

$$R = i \cot(kh\sqrt{\varepsilon_{Ag}}/2)/(2\sqrt{\varepsilon_{Ag}}), \quad (3)$$

$$Q = i\sqrt{\varepsilon_{Ag}} \cot(kh\sqrt{\varepsilon_{Ag}}/2)/2, \quad (4)$$

which contain the strip characteristics such as electric thickness  $kh$  and  $\varepsilon_{Ag}$ ,  $\vec{n}$  is the unit vector normal to the strip, and the superscripts  $\pm$  denote the limit values of the field at the top and bottom faces of the strip, respectively. These GBC are valid if  $|kh| \ll 1$  and  $|\varepsilon_{Ag}| \gg 1$  [22], [23].

GBC (1)–(2) enables one to exclude from consideration the inner domain of thin strip at the expense of the introduction of more complicated conditions at the strip median line  $S$  (see [22], [23]). As GBC are derived originally for infinite thin material sheet, and we consider a finite strip with sharp edges, we have to complement the formulation with the local power finiteness condition. Full validation of GBC in the metal nanostrip scattering in the optical range was published in [23].

Note that thanks to the fact that the natural (eigenvalue) frequency is real-valued at the threshold, it suffices to use the Sommerfeld radiation condition at infinity. This removes the exponential growth of the mode field at infinity – now it decays as a usual cylindrical wave.

The last condition (vi) follows from the considered nanolaser configuration. It enables splitting all natural modes into four independent classes of symmetry with respect to the  $x$  and  $y$ -axes:  $x$ -even/ $y$ -even case ( $EE$ ),  $x$ -even/ $y$ -odd case ( $EO$ ),  $x$ -odd/ $y$ -odd case ( $OO$ ), and  $x$ -odd/ $y$ -even case ( $OE$ ). This greatly improves the stability of the iterative search for eigenvalues, as it prevents the algorithm from hopping to a closely located eigenvalue belonging to a different symmetry class.

### B. Symmetry-Adapted Green's Functions

To meet the conditions 1) and 2) and also the radiation condition 4), the field function  $H_z^{ij}(\vec{r})$  ( $i, j = E, O$ ) can be sought as a sum of the convolutions of the unknown effective electric and magnetic current functions  $v_{ij}(\vec{r})$  and  $w_{ij}(\vec{r})$ , with the Green's function and its normal derivative, respectively. Here, in order to perform the mentioned above splitting into four classes of symmetry, the Green's functions are subjected to the condition

(vi) in one of four possible forms,

$$H_z^{ij}(\vec{r}_0) = k_\nu \int_S v_{ij}(\vec{r}) G_{ij} d\vec{r} + \int_S w_{ij}(\vec{r}) \frac{\partial G_{ij}}{\partial \vec{n}(\vec{r})} d\vec{r}, \quad (5)$$

$$G^{ij}(\vec{r}, \vec{r}_0) = \begin{cases} G_0^{ij}(\vec{r}, \vec{r}_0) + G_{shell}^{ij}(\vec{r}, \vec{r}_0), & r, r_0 < a \\ G_{shell}^{ij}(\vec{r}, \vec{r}_0), & r < a < r_0 \end{cases}, \quad (6)$$

where  $k_\nu = k\nu$  ( $r_0 < a$ ) or  $k$  ( $r_0 > a$ ).

In these expressions, the functions  $G_0^{ij}(r, r_0)$  are the 2D free-space Green functions and  $G_{shell}^{ij}(r, r_0)$  are the terms accounting for the presence of the circular QWR in the H-polarization case. Depending on the class of symmetry, these symmetry-adapted Green's functions are given as follows:

*EE/EO-case*

$$G_0^{EE/EO} = \frac{i}{16} [H_0(k\nu r_{EE}) + H_0(k\nu r_{OE}) \pm H_0(k\nu r_{EO}) \pm H_0(k\nu r_{OO})], \quad (7)$$

$$G_{shell}^{EE/EO} = \frac{i}{16} \sum_{n=-\infty}^{\infty} J_n(k\nu r) \begin{cases} C_n J_n(k\nu r_0), & r_0 < a \\ B_n H_n(kr_0), & r_0 > a \end{cases} \times \eta_n^\pm (e^{in\varphi_0} \pm e^{-in\varphi_0}) e^{-in\varphi}, \quad (8)$$

$$r_{EE/EO} = \sqrt{(x - x_0)^2 + (y \mp y_0)^2}; \quad (9)$$

*OE/OO-case*

$$G_0^{OE/OO} = \frac{i}{16} [H_0(k\nu r_{EE}) - H_0(k\nu r_{OE}) \pm H_0(k\nu r_{EO}) \mp H_0(k\nu r_{OO})], \quad (10)$$

$$G_{shell}^{OE/OO} = \frac{i}{16} \sum_{n=-\infty}^{\infty} J_n(k\nu r) \begin{cases} C_n J_n(k\nu r_0), & r_0 < a \\ B_n H_n(kr_0), & r_0 > a \end{cases} \times \eta_n^\mp (e^{in\varphi_0} \pm e^{-in\varphi_0}) e^{-in\varphi}, \quad (11)$$

$$r_{OE/OO} = \sqrt{(x + x_0)^2 + (y \mp y_0)^2}. \quad (12)$$

Here,  $\eta_n^\pm = 1 \pm (-1)^n$ , while  $H_n(\cdot) = H_n^{(1)}(\cdot)$ , and  $D_n, C_n$  and  $B_n$  are known coefficients:

$$D_n = H_n'(ka) J_n(k\nu a) - \nu^{-1} J_n'(k\nu a) H_n(ka), \quad (13)$$

$$C_n = D_n^{-1} [\nu^{-1} H_n'(k\nu a) H_n(ka) - H_n'(ka) H_n(k\nu a)], \quad (14)$$

$$B_n = D_n^{-1} \nu^{-1} [H_n'(k\nu a) J_n(k\nu a) - J_n'(k\nu a) H_n(k\nu a)]. \quad (15)$$

### C. Singular Integral Equations and Their Discretization

By substituting the field representations (5) into GBC (1)–(2), each of considered four boundary-value problems is reduced to equivalent singular or hyper-singular IEs (depending on the class of symmetry):

*EO-case*

$$8Rw(x_0) + \int_{-d}^d w(x) \left[ \frac{H_1(k\nu r_{EO})}{r_{EO}} + \frac{H_1(k\nu r_{OE})}{r_{OE}} \right] dx + \int_{-d}^d w(x) \sum_{n=-\infty}^{\infty} n^2 \eta_n^- \text{sign}(x^{n-1} x_0^{n-1}) \frac{\chi_n(x, x_0)}{|xx_0|} = 0 \quad (16)$$

*EE-case*

$$8Qv(x_0) + k\nu \int_{-d}^d v(x) [H_0(k\nu r_{EE}) + H_0(k\nu r_{OE})] dx + k\nu \int_{-d}^d v(x) \sum_{n=-\infty}^{\infty} \eta_n^+ \text{sign}(x^n x_0^n) \chi_n(x, x_0) = 0 \quad (17)$$

*OO-case*

$$8Rw(x_0) + \int_{-d}^d w(x) \left[ \frac{H_1(k\nu r_{EE})}{r_{EE}} - \frac{H_1(k\nu r_{OO})}{r_{OO}} \right] dx + \int_{-d}^d w(x) \sum_{n=-\infty}^{\infty} n^2 \eta_n^+ \text{sign}(x^{n-1} x_0^{n-1}) \frac{\chi_n(x, x_0)}{|xx_0|} = 0 \quad (18)$$

*OE-case*

$$8Qv(x_0) + k\nu \int_{-d}^d v(x) [H_0(k\nu r_{EO}) - H_0(k\nu r_{OE})] dx + k\nu \int_{-d}^d v(x) \sum_{n=-\infty}^{\infty} \eta_n^- \text{sign}(x^n x_0^n) \chi_n(x, x_0) = 0 \quad (19)$$

where  $\chi_n(x, x_0) = C_n J_n(k\nu|x|) J_n(k\nu|x_0|)$ . In order to avoid the bulky notations, we have omitted in the above formulas the corresponding symmetry indices of the current functions  $v_{ij}(\cdot)$  and  $w_{ij}(\cdot)$ .

Symmetry-adapted IEs (16)–(19) can be discretized by various numerical techniques so that instead of them we obtain matrix equations,  $\mathbf{A}^{EE/OE} \mathbf{V}^{EE/OE} = 0$  and  $\mathbf{A}^{EO/OO} \mathbf{W}^{EO/OO} = 0$ . Keeping in mind the condition (v) and the edge behavior of the unknown functions, we use Nystrom discretization with the aid of specially tailored quadrature formulas of interpolation type. Here the order of the discrete analog of IE (i.e., the size of the matrix) is determined by the power  $N$  of the trigonometric polynomial, which approximates the unknown surface-current function. The convergence of the approximate solutions to the accurate ones with  $N \rightarrow \infty$  is guaranteed by the theorems on the quadratures [24] and hence the accuracy of computations is easily controlled by adapting  $N$ . Note that, in sharp contrast to other numerical techniques and to commercial codes, the accuracy can be brought to machine precision if  $N$  is only reasonably larger than the optical size of the strip, i.e., its width in terms of the surface-plasmon wave length.

Following [24]–[27], we use for IEs (16) and (18) the Gauss-Chebyshev quadrature formulas of the  $N$ -th order (with the Chebyshev weight  $\sqrt{1-t^2}$ ), with nodes in the nulls of the Chebyshev polynomials of the second kind,  $t_j = \cos(\pi j/N)$ ,  $j = 1, \dots, N$ . While for IEs (17) and (19), we use the Gauss-

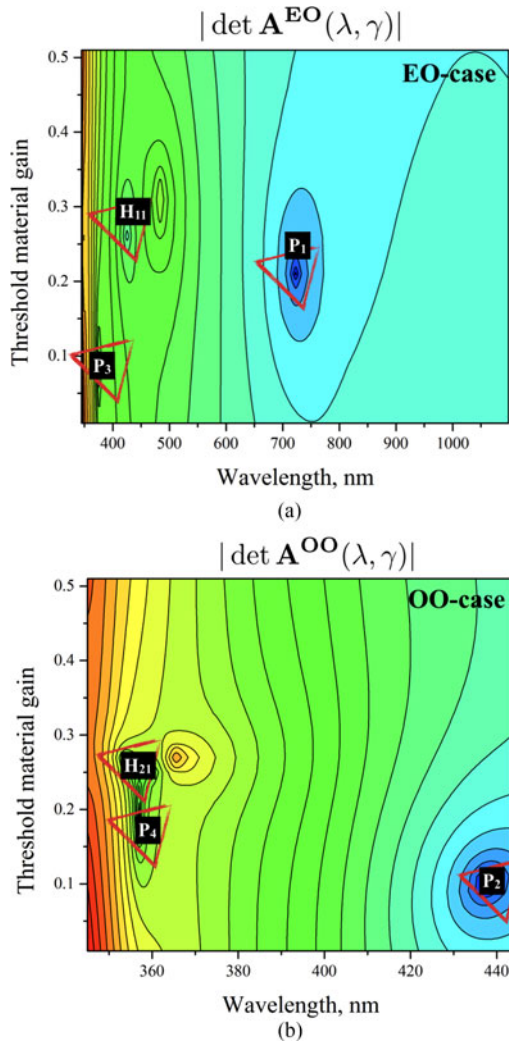


Fig. 2. The maps of two determinants,  $\det \mathbf{A}^{EO}(\lambda, \gamma)$  (a) and  $\det \mathbf{A}^{OO}(\lambda, \gamma)$  (b) as a function of the wavelength and threshold gain for a strip nanolaser of  $150 \times 30 \text{ nm}^2$  placed into QWR of the radius 200 nm.

Legendre quadrature formulas of the  $m$ -th order with nodes in the nulls of Legendre polynomials  $P_N(\tau_j) = 0$ ,  $j = 1, \dots, N$ .

#### D. Search for LEP Eigenvalues

Finally, search for non-trivial solutions of (16)–(19) reduces to solving four independent determinantal equations  $\det \mathbf{A}^{ij}(\lambda, \gamma) = 0$  for  $i, j = E, O$ , which are LEP characteristic equations. For accurate computation of the lasing spectra and the associated threshold values of gain in QWR we apply modified hybrid Powell algorithm of the IMSL library. This is an iterative algorithm, which needs certain initial guess values.

In order to find good initial guesses, we plot at first the map of the corresponding determinant as a function of  $\lambda$  and  $\gamma$  in the wavelength range from 300 nm to 900 nm and threshold gain range from  $10^{-6}$  to 0.5. As an example, we show in Fig. 2 two maps of determinants for the modes of the  $EO$  and  $OO$  classes of symmetry of a nanolaser made of silver strip of  $150 \times 30 \text{ nm}^2$  placed into QWR of the radius of 200 nm. Each map reveals a number of local minima. The initial guesses for the LEP

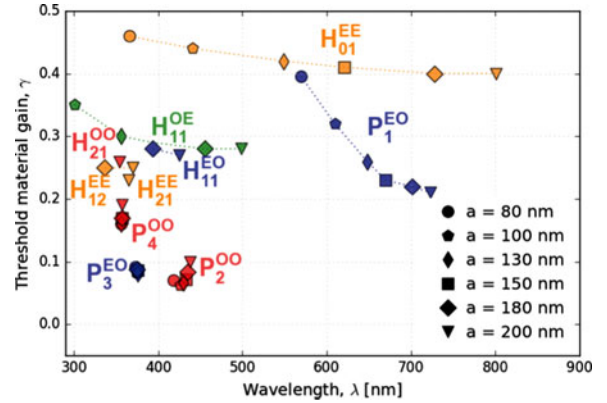


Fig. 3. Migration of the LEP modes of a strip nanolaser ( $150 \times 30 \text{ nm}^2$ ,  $\alpha = 1.5$ ) with the growth of the QWR radius from 80 to 200 nm.

eigenvalues are taken from those minima, where determinant is close to zero. Then they are calculated by iterations until the machine precision is reached. Note that the minima containing the eigenvalues are well separated from each other within the same class of symmetry. This is not so if we compare two maps in Fig. 2 for the modes of different classes. Therefore any algorithm built without the separation is prone to unstable behavior, and working with each class. Therefore any algorithm built without the separation is prone to unstable behavior, and working with each class separately, despite the efforts needed to derive analytical expressions like (16)–(19), is truly beneficial.

### III. NUMERICAL RESULTS

When analyzing the LSP lasing modes of the silver-strip nanolaser, it is interesting, first of all, to design what can be called a single-mode plasmon-assisted nanolaser, i.e., a device having the working mode essentially separated, in wavelength and in threshold gain, from the other modes. Here we keep in mind our previous numerical studies on the plane wave scattering by the noble-metal strips in the free space [24]–[27] and immersed in a dielectric circular shell (see Appendix). The results of these studies suggest that in the context of the electromagnetic engineering of a plasmon-assisted nanolaser, it makes sense considering neither very narrow nor very thin silver nanostrips. Taking this into account, we take its cross-section as  $150 \times 30 \text{ nm}^2$ .

#### A. Choice of the Model of Dielectric Permittivity of Silver

There is no need to emphasize that the choice of the dielectric function or refractive index of silver in the optical range is extremely important. In our analysis we prefer using the experimental data of [28] for the silver permittivity instead of the well-known Drude approximation or even the formulas proposed as its improvements, namely Drude in combination with the Lorentz-pole pairs or two critical points [29]. The reason is that the former is heavily erroneous in the violet part of the visible-light spectrum especially in terms of the absorption, and the latter shows negative losses in silver at certain wavelengths – see [4] for a detail investigation.

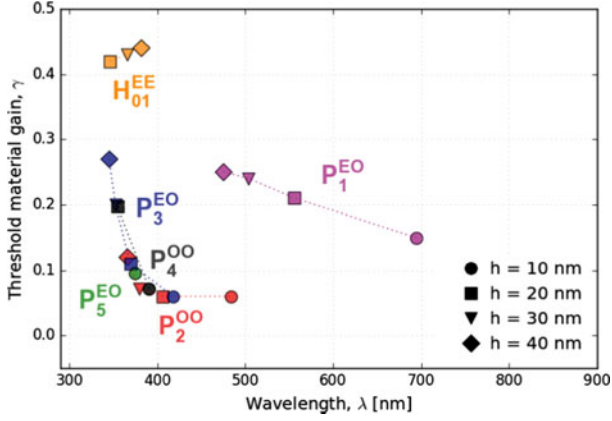


Fig. 4. Migration of the LEP modes of a strip ( $100 \times h \text{ nm}^2$ ,  $\alpha = 1.5$ ) placed into QWR of the radius of 80 nm with the growth of the strip thickness from 10 to 40 nm.

### B. Cocktail of Lasing Modes

As mentioned, in order to find the nanostrip-in-QWR laser modes emitting in the visible range, we solve determinantal equations obtained after the discretization of (16)–(19).

The computed results are collected in Figs. 3 and 4, where we show the part of the  $(\lambda, \gamma)$  plane corresponding to the visible range. Here, the modes of different symmetry classes are presented with different-color symbols. The considered nanostrip laser can emit visible light on several LSP modes  $P_m$  with  $m = 1, 2, 3, 4$  and also on the lowest shell modes  $H_{01}, H_{11}$ , and some others, depending on the QWR radius. Note that the shell modes are in fact the microcavity polaritons slightly perturbed by the presence of strip.

In Fig. 3 we show also the trajectories of migration of the LEP eigenvalues (i.e., emission wavelengths and associated thresholds) under the variation of the radius of QWR from 80 nm (“thin QW”) to 200 nm (“thick QWR”). In Table I we present the found LEP eigenvalues for the same modes with better precision, for four values of QWR radius (though only three digits are shown).

As one can see, if the QWR diameter is close to the strip width (e.g.,  $2a = 160 \text{ nm}$  and  $2d = 150 \text{ nm}$ ), then the principal LSP mode  $P_1$  has the largest emission wavelength of 570

nm and the threshold material gain of 0.395. Besides of them, the first shell mode  $H_{01}^{EE}$  appears at the wavelength of around 300 nm, having large threshold value around 0.5.

Note that the higher-order plasmon modes  $P_2$  and  $P_3$  demonstrate noticeably lower threshold values than their principal sister-mode  $P_1$ , namely 0.07 and 0.093 in the thin-QWR case. This is explained by smaller dissipation losses thanks to the additional nulls of electric field along the strip width. At the same time, higher-order plasmons are considerably blue-shifted so that the mentioned reduction of threshold is corrupted by the larger bulk losses in silver in the violet range. As a result, the threshold of  $P_4$  shows larger value than of  $P_3$ .

If the QWR radius varies from 80 nm to 200 nm, then all the shell modes and the lowest-order LSP mode  $P_1$  get red-shifted in the wavelength. Besides, such a change in QWR radius brings as many as five new shell modes to the visible range. At the same time, the LSP modes of the higher orders ( $P_2, P_3$  and  $P_4$ ) remain approximately at the same wavelengths in the violet range. As regards the thresholds, we observe that the shell-mode thresholds slightly decrease if the QWR radius increases, apparently because of reduced radiation leakage.

However the thresholds of the plasmon modes behave in different manner depending on their indices and the classes of symmetry. Namely, the threshold gain of the plasmon mode of the  $EO$ -class,  $P_3$ , slightly decreases with increasing the QWR radius. In the contrary, the threshold gain of the principal LSP mode  $P_1$  of the  $EO$ -class drops almost twice lower, from 0.395 to 0.21. At the same variation of the QWR radius, the thresholds of the even-index plasmon modes (i.e.,  $P_2$  and  $P_4$ ) increase slightly.

Correct identification of modes in the above presented cocktail calls for the visualization of the corresponding near-field patterns. The magnetic field,  $|H_z^{ij}(r)|$  for each class of symmetry  $j = E, O$  is defined by the Equations (20)–(23) as shown at the bottom of this page, where  $r = d\rho$ , and  $\kappa = k_\nu d$ , and  $\{A_l\}_{l=1}^N$  are the Legendre weight coefficients of the  $N$ -th order,  $A_l = 2 / ((1 - \tau_j^2) P'_N(\tau_j)^2)$ .

In Fig. 5, we present the near and far-field portraits of all visible-range LEP modes for the nanostrip of  $150 \times 30 \text{ nm}^2$  placed in QWR shell of the radius  $a = 200 \text{ nm}$ , which is more than 2.5 times larger than the strip half width.

$$H_z^{EO/OO}(t_x, t_y) = \frac{\pi}{8(N+1)} \sum_{l=1}^N w(t_l)(1 - t_l^2) \left\{ \begin{array}{l} \sum_{n=1}^{\infty} B_n \zeta_n^{\pm}(t_l) H_n(\kappa \rho_0), r_0 > a \\ \sum_{n=1}^{\infty} C_n \zeta_n^{\pm}(t_l) J_n(\kappa \rho_0) + i \kappa t_y \left[ \frac{H_1(\kappa \rho^{EO})}{\rho^{EO}} \pm \frac{H_1(\kappa \rho^{OO})}{\rho^{OO}} \right], r_0 < a \end{array} \right\} \quad (20)$$

$$H_z^{EE}(t_x, t_y) = \frac{i\kappa}{8} \sum_{l=1}^N A_l v(\tau_l) \left\{ \begin{array}{l} 2B_0 H_0(\kappa \rho_0) J_0(\kappa \nu |\tau_l|) + \sum_{n=1}^{\infty} B_n \xi_n^+ H_n(\kappa \rho_0), r_0 > a \\ 2C_0 J_0(\kappa \rho_0) J_0(\kappa |\tau_l|) + \sum_{n=1}^{\infty} C_n \xi_n^+ J_n(\kappa \rho_0) + H_0(\kappa \nu \rho^{EE}) + H_0(\kappa \nu \rho^{OE}), r_0 < a \end{array} \right\} \quad (21)$$

$$H_z^{OE}(t_x, t_y) = \frac{i\kappa}{8} \sum_{l=1}^N A_l v(\tau_l) \left\{ \begin{array}{l} \sum_{n=1}^{\infty} B_n \xi_n^- H_n(\kappa \rho_0), r_0 > a \\ \sum_{n=1}^{\infty} C_n \xi_n^- J_n(\kappa \rho_0) + H_0(\kappa \rho^{EE}) - H_0(\kappa \rho^{OE}), r_0 < a \end{array} \right\} \quad (22)$$

$$\zeta_n^{\pm}(t_l) = n J_n(\kappa |t_l|) \frac{\text{sign}(t_l)^{n-1}}{|t_l|} \eta_n^{\pm}(e^{in\varphi_0} - e^{-in\varphi_0}), \quad \xi_n^{\pm}(\tau_l) = J_n(\kappa \nu |\tau_l|) \text{sign}(\tau_l)^n \eta_n^{\pm}(e^{in\varphi_0} + e^{-in\varphi_0}). \quad (23)$$

TABLE I  
EIGENMODE WAVELENGTH AND THRESHOLD MATERIAL GAIN FOR A NANOSTRIP LASER ( $150 \times 30 \text{ nm}^2$ ,  $\alpha = 1.5$ )

QW (nm)	Classes of symmetry			
	EO	OO	OE	EE
	Eigenmode wavelength and threshold: $(\lambda(\text{nm}), \gamma)$			
80	$P_1$ (569.69, 0.395) $P_3$ (373.09, 0.093)	$P_2$ (418.02, 0.07) $P_4$ (356.67, 0.17)	....	$H_{01}$ (365.59, 0.46)
100	$P_1$ (609.42, 0.32) $P_3$ (374.6, 0.084)	$P_2$ (425.38, 0.062) $P_4$ (356.93, 0.17)	$H_{11}$ (300.9, 0.35)	$H_{01}$ (440.4, 0.44)
150	$P_1$ (669.98, 0.23) $P_3$ (375.5, 0.086)	$P_2$ (432.18, 0.072) $P_4$ (356.93, 0.17)	$H_{11}$ (393.73, 0.28)	$H_{01}$ (620.46, 0.41)
200	$P_1$ (722.69, 0.21) $P_3$ (375.21, 0.082) $H_{11}$ (424.8, 0.27)	$P_2$ (437.59, 0.1) $P_4$ (356.89, 0.19) $H_{21}$ (354.17, 0.26)	$H_{11}$ (498.84, 0.29)	$H_{01}$ (800.08, 0.4) $H_{21}$ (369.75, 0.25) $H_{12}$ (364.8, 0.23)

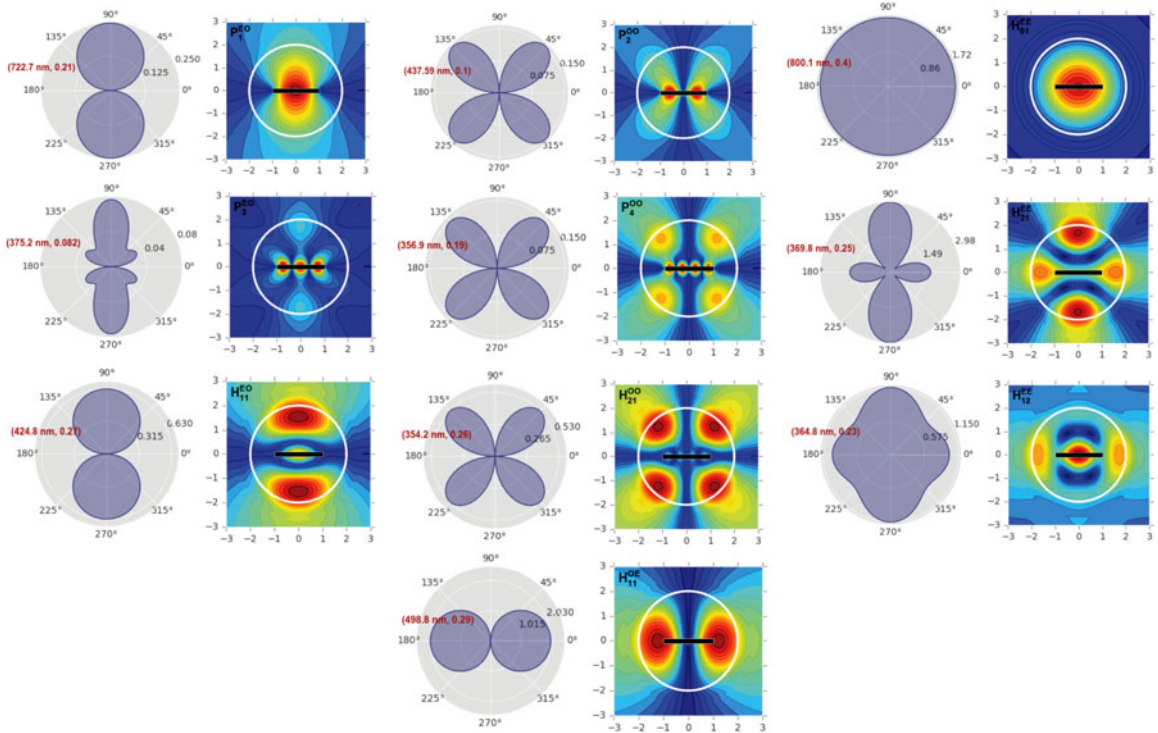


Fig. 5. Near and far field portraits for the H-polarized lasing modes of the  $150 \times 30 \text{ nm}^2$  silver strip nanolaser placed into QWR of 200 nm radius.

In such a thick QWR, the  $P_3$  mode has the lowest material-gain threshold of 0.082 followed by the nearby sister-mode  $P_2$  with 0.10, while for the lowest-threshold shell mode  $H_{12}^{EE}$  it is 0.23, which is more than 2 times larger.

In the case of thick QWR, the principal plasmon mode  $P_1$  has moderate threshold of 0.23 and remains well-distanced from higher-order modes of all types in wavelength (723 nm) except of the lowest shell mode  $H_{01}^{EE}$  (800 nm), which has much higher threshold of 0.41.

In Fig. 4, we present the trajectories of the LEP eigenvalues on the plane  $(\lambda, \gamma)$  for the nanostrip-in-QWR laser with  $a = 80 \text{ nm}$  and silver strip width  $2d = 150 \text{ nm}$ , corresponding to the variation of the strip thickness  $h$  from 10 nm to 40 nm. As expected, on the thin strip the principal plasmon mode  $P_1$  is

well red-shifted to 700 nm while higher-order plasmons are in the blue and violet bands. Making strip thicker shifts  $P_1$  to the green light and higher plasmons to the ultra-violet. Note that the first shell mode  $H_{01}^{EE}$  keeps its position in ultra-violet thanks to rather small diameter of QWR.

#### IV. CONCLUSION

We have investigated the wave emission spectrum of a plasmonic silver nanostrip placed into a circular QWR, in the visible-light range. To the best of our knowledge, this work is the first to consider such a nanolaser and demonstrate how to design it in optimal way. The modified eigenvalue problem or LEP, which we use, is adapted to extract the mode threshold in addition

to the emission wavelength. It is formulated in mathematically grounded manner and fully takes into account the presence and the shape of the active region. We have reduced it to four independent IEs and further to determinantal equations, which provide guaranteed convergence and are free of the spurious eigenvalues. This algorithm is a powerful, economic and trusted numerical instrument, able, if desired, to deliver the results as accurate as machine precision.

The obtained results of the LEP analysis show that the considered nanostrip-in-QWR laser can emit visible light on the LSP modes  $P_m, m = 1, 2, 3, 4$  and also on the lowest shell modes, which can be viewed as QWR polariton modes slightly perturbed by the strip. The threshold gains and the emission wavelengths of the principal LSP mode  $P_1$  and the shell modes strongly depend on the QWR radius and the refractive indices of QWR and the host medium. The lowest thresholds are found for the higher-order LSP modes  $P_2$  and  $P_3$  which are emitting in the ultra-violet while the principal plasmon  $P_1$  is significantly red-shifted.

Summarizing, in order to rarefy the lasing mode spectrum and create conditions for a single-mode operation, the QWR diameter should be only slightly larger than the metal strip width. In such case, the shell modes are either blue-shifted out of the visible range, or obtain high thresholds because of the larger losses in silver in the ultra-violet band. Then the principal plasmon mode  $P_1$  remains alone in the green or yellow part of the visible range and still keeps a reasonable threshold.

Another option for the single-mode operation is to work with one of the higher-order LSP modes  $P_2$  or  $P_3$  that have twice lower thresholds than the principal LSP mode  $P_1$  and 5 times lower than the first shell mode  $H_{01}^{EE}$ .

We would like to add that the considered above nanostrip-in-QWR laser model can be sophisticated further, to take into account certain fine details. For example, it is known that attachment of gain material to metal leads to the bleaching of the adjacent layer of the former. This can be incorporated into the modeling via introduction of flat-layered structure of the nanostrip, now with metal core sandwiched between two thin layers of dielectric without the gain  $\gamma$ . Then expressions (3) and (4) for the electric and magnetic resistivities must be replaced by their analogues found using the approach of [30].

In this work, we have computed various configurations based on silver strips of 100 nm and 150 nm widths that provided the location of principal LSP mode in the visible range. By taking wider strips one can shift it to mid-infrared. Our model and algorithm are equally good to compute such wider strips. Still one should keep in mind that in that case the QWR will have even larger cross-sectional dimensions and, strictly speaking, the whole device will loose an honor to be called a nanolaser.

## APPENDIX

### PLANE-WAVE SCATTERING BY A METAL PLASMONIC STRIP PLACED INTO A CIRCULAR DIELECTRIC ROD

#### A. Basic Formulas

In the case of the time-harmonic plane-wave scattering by a metal plasmonic strip placed into a dielectric rod (see Fig. 6),

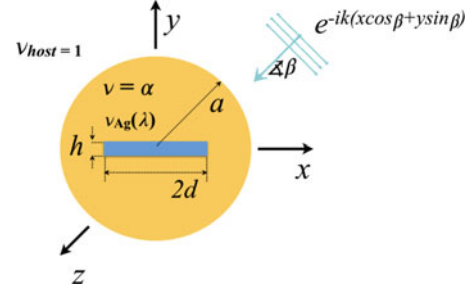


Fig. 6. Cross-sectional geometry of the plane wave scattering by a flat nanostrip placed into a dielectric circular cylinder.

there is no iterative search for eigenvalues. Instead, we have to find the scattered field as a function of the given (real) frequency and other parameters. Hence we do not need to split the problem into four classes of symmetry. This means that a pair of decoupled IEs can be derived using the conventional Green's function of the 2D free space with a circular dielectric inclusion, i.e., neglecting the two-fold symmetry conditions. Such IEs, with non-zero right-hand parts are as follows:

$$4Rv(x_0) + k_\nu \int_{-d}^d v(x) H_0(k_\nu |x - x_0|) dx + k_\nu \int_{-d}^d v(x) \sum_{n=-\infty}^{\infty} \text{sign}(x^n x_0^n) \chi_n(x, x_0) dx = 4iU_0^{-1}, \quad (24)$$

$$4Qw(x_0) + \int_{-d}^d w(x) \frac{H_1(k_\nu |x - x_0|)}{|x - x_0|} dx + \int_{-d}^d w(x) \sum_{n=-\infty}^{\infty} n^2 \text{sign}(x^{n-1} x_0^{n-1}) \frac{\chi_n(x, x_0)}{|xx_0|} dx = -4(ik)^{-1} \partial U_0^{-1} / \partial \vec{n}(\vec{r}_0), \quad (25)$$

where  $U_0$  is the field induced by the incident plane wave in the absence of the strip while  $U_0^{in}$  is the plane wave field (while  $\beta$  is the incidence angle, see Fig. 6),

$$U_0 = \begin{cases} U_0^-, & r_0 < a \\ U_0^{in} + U_0^+, & r_0 > a \end{cases}, \quad (26)$$

$$U_0^- = \sum_{n=-\infty}^{\infty} (-i)^n C_n J_n(k_\nu r_0) e^{in(\varphi_0 - \beta)}, \quad (27)$$

$$U_0^{in} = \sum_{n=-\infty}^{\infty} (-i)^n J_n(kr_0) e^{in(\varphi_0 - \beta)}, \quad (28)$$

$$U_0^+ = \sum_{n=-\infty}^{\infty} B_n H_n(kr_0) e^{in\varphi_0}, \quad (29)$$

and coefficients  $B_n$  and  $C_n$  are given in (14) and (15), respectively. To solve these IEs numerically we use the same Nystrom-type discretization as in Section II-C with the aid of specially tailored quadrature formulas of interpolation type.

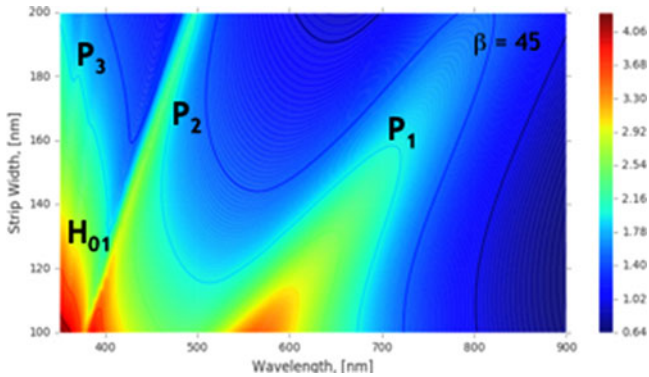


Fig. 7. The map of the normalized TSCS as a function of  $\lambda$  and  $2d$  for the silver nanostrip of thickness  $h = 30$  nm placed in the dielectric rod of radius  $a = 200$  nm and refractive index  $\alpha = 1.5$ . The angle of incidence of plane wave is  $\beta = \pi/4$ .

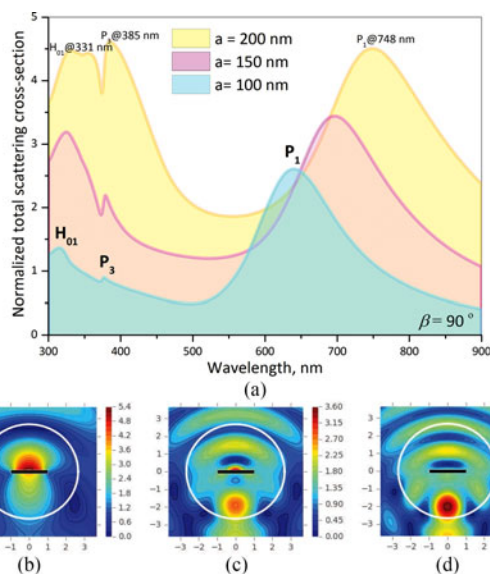


Fig. 8. (a) Normalized TSCS as a function of the wavelength for the strip of  $150 \times 30$  nm<sup>2</sup> placed in a dielectric rod of  $a = 100, 150$  and  $200$  nm (normal incidence,  $\beta = \pi/2$ ). Near-field portraits in four resonances for the same rod radius of  $200$  nm:  $P_1$  at  $748$  nm (b),  $P_3$  at  $385$  nm (c), and  $H_{01}$  at  $331$  nm (d).

### B. Scattering Resonances on LSP and Shell Modes

As known, the number of the LSP resonances excited on the strip in the visible range, their wavelengths and Q-factors significantly depend on the strip thickness and its width [25]–[27]. In general, the thinner the strip, the larger the number of LSP resonances excited within the visible range.

However, if the strip gets wider, all plasmons are red-shifted that entails lower thresholds because of smaller bulk losses in silver. As follows from Figs. 7 and 8(a), this also applies to the resonances on LSP modes in the plane-wave scattering by a silver nanostrip placed in a dielectric rod.

In Fig. 7, the relief of the TSCS as a function of the wavelength and the strip width is presented for the silver strip of  $2d \times 30$  nm<sup>2</sup> placed in the silica rod ( $\alpha = 1.5$ ) of the radius  $a = 200$  nm ( $\beta = \pi/4$ ). Here, apart from plasmon resonances, one can detect the resonance on the first shell mode  $H_{01}$ , which appears in the ultra-violet.

It is obvious that number and the wavelengths of the shell modes depend also on the contrast between the refractive indices of the rod and the host medium. If the contrast gets larger, then other shell modes enter the visible range and resonances on them complicate the optical response of the strip-in-rod scatterer even further. As one can see from Fig. 8(a), with increasing the dielectric rod radius  $a$  from  $100$  nm to  $200$  nm, the higher-order LSP resonance  $P_3$  remains almost at the same place in the violet range. In contrast, the resonance on the principal plasmon mode  $P_1$  red-shifts in wavelength. Only one shell-mode resonance,  $H_{01}$ , is observed in the ultra-violet range, appearing even if the shell radius is as small as  $100$  nm. For the thicker rods, e.g. if  $a = 200$  nm, the wavelength of the  $H_{01}$  mode gets closer to that of  $P_3$ . As a result the TSCS peak splits to two equal summits at  $331$  nm and  $385$  nm. Visualization of the near-field patterns at these wavelengths demonstrates hot spots of both  $P_3$  and  $H_{01}$  modes – see panels (c) and (d). Note that these two modes cannot hybridize as they belong to two different classes of symmetry,  $EO$  and  $EE$  – see Table I.

Which of the resonances, of the full cocktail of the LSP and shell modes, appear as peaks on the visible-range spectra of TSCS and absorption cross-section depends also on the angle of incidence. As explained in Section II, each mode belongs to certain class of symmetry with respect to the  $x$  and  $y$  axes. Therefore in the normal ( $\beta = \pi/2$ ) and on-edge ( $\beta = 0$ ) incidence cases some of the modes give no response because of their fields orthogonality to the incident wave.

### REFERENCES

- [1] M. A. Noginov, G. Zhu, and A. M. Belgrave, “Demonstration of a spaser-based nanolaser,” *Nature*, vol. 460, pp. 1110–1112, 2009.
- [2] Q.-F. Yao *et al.*, “Analysis of mode coupling and threshold gain control for nanocircular resonators confined by isolation and metallic layers,” *J. Lightw. Technol.*, vol. 31, no. 5, pp. 786–792, Mar. 2013.
- [3] L. Tang, H. Shi, H. Gao, J. Du, and Z. Zhang, “An eigenvalue method to study the threshold behaviors of plasmonic nano-lasers,” *Appl. Phys. B: Lasers Opt.*, vol. 113, pp. 575–579, 2013.
- [4] D. M. Natarov, “Modes of a core-shell silver wire plasmonic nanolaser beyond the Drude formula,” *IOP J. Opt.*, vol. 16, 2014, Art. no. 075002.
- [5] F. van Beijnum *et al.*, “Surface plasmon lasing observed in metal hole arrays,” *Phys. Rev. Lett.*, vol. 110, 2013, Art. no. 206802.
- [6] W. Zhou *et al.*, “Lasing action in strongly coupled plasmonic nanocavity arrays,” *Nature Nanotechnol.*, vol. 8, pp. 506–511, 2013.
- [7] A. H. Schokker and A. F. Koenderink, “Lasing at the band edges of plasmonic lattices,” *Phys. Rev. B*, vol. 90, no. 15, 2014, Art. no. 15545225.
- [8] A. Yang *et al.*, “Real-time tunable lasing from plasmonic nanocavity arrays,” *Nature Commun.*, vol. 6, 2015, Art. no. 6939.
- [9] V. O. Byelobrov, T. M. Benson, and A. I. Nosich, “Binary grating of sub-wavelength silver and quantum wires as a photonic-plasmonic lasing platform with nanoscale elements,” *IEEE J. Sel. Topics Quantum Electron.*, vol. 18, no. 6, pp. 1839–1846, Nov/Dec. 2012.
- [10] B. Ji *et al.*, “Non-blinking quantum dot with a plasmonic nanoshell resonator,” *Nature Nanotechnol.*, vol. 10, pp. 170–175, 2015.
- [11] E. I. Smotrova *et al.*, “Optical theorem helps understand thresholds of lasing in microcavities with active regions,” *IEEE J. Quantum Electron.*, vol. 47, no. 11, pp. 20–30, Jan. 2011.
- [12] E. I. Smotrova *et al.*, “Spectra, thresholds and modal fields of a kite-shaped microcavity laser,” *J. Opt. Soc. Amer. B*, vol. 40, no. 6, pp. 1732–1742, 2013.
- [13] E. I. Smotrova and A. I. Nosich, “Optical coupling of an active microdisk to a passive one: Effect on the lasing thresholds of the whispering-gallery supermodes,” *Opt. Lett.*, vol. 38, no. 12, pp. 2059–2061, 2013.

- [14] A. O. Spiridonov, E. M. Karchevskii, and A. I. Nosich, "Symmetry accounting in the integral-equation analysis of the lasing eigenvalue problems for two-dimensional optical microcavities," *J. Opt. Soc. Amer. B*, vol. 34, no. 7, pp. 1435–1443, 2017.
- [15] S. Nojima, "Theoretical analysis of feedback mechanisms of two-dimensional finite-sized photonic-crystal lasers," *J. Appl. Phys.*, vol. 98, no. 4, 2005, Art. no. 043102.
- [16] A. Mock, "First principles derivation of microcavity semiconductor laser threshold condition and its application to FDTD active cavity modeling," *J. Opt. Soc. Amer. B*, vol. 27, no. 11, pp. 2262–2272, 2010.
- [17] S. W. Chang, "Confinement factors and modal volumes of micro- and nanocavities invariant to integration regions," *IEEE J. Sel. Topics Quantum Electron.*, vol. 18, no. 6, pp. 1771–1780, Nov./Dec. 2012.
- [18] D. Gagnon, J. Dumont, J.-L. Deziel, and L. J. Dubé, "Ab initio investigation of lasing thresholds in photonic molecules," *J. Opt. Soc. Amer. B*, vol. 31, no. 8, pp. 1867–1873, 2014.
- [19] O. V. Shapoval, "Electromagnetic engineering of a plasmon-strip loaded quantum wire," in *Proc. Int. Conf. Electron. Nanotechnol.*, 2016, pp. 154–156.
- [20] O. V. Shapoval, "Basic equations of LEP for a silver strip nanolaser," in *Proc. Int. Conf. Electron. Nanotechnol.*, 2015, pp. 222–224.
- [21] O. V. Shapoval, D. Natarov, and K. Kobayashi, "Wave scattering and emission by a plasmonic strip placed into a circular quantum wire," in *Proc. Int. Young Sci. Forum Appl. Phys. Eng.*, 2016, pp. 187–189.
- [22] E. Bleszynski, M. Bleszynski, and T. Jaroszewicz, "Surface-integral equations for electromagnetic scattering from impenetrable and penetrable sheets," *IEEE Antenna Propag. Mag.*, vol. 35, no. 6, pp. 14–25, Dec. 1993.
- [23] I. O. Sukharevsky, O. V. Shapoval, A. I. Nosich, and A. Altintas, "Validity and limitations of the median-line integral equation technique in the scattering by material strips of sub-wavelength thickness," *IEEE Trans. Antennas Propag.*, vol. 62, no. 7, pp. 3623–3631, Jul. 2014.
- [24] O. V. Shapoval, "Scattering of light waves by finite metal nanostrip gratings: Nystrom-type method and resonance effects," *Radioelectronics Commun. Syst.*, vol. 58, no. 5, pp. 201–211, 2015.
- [25] O. V. Shapoval, R. Sauleau, and A. I. Nosich, "Modeling of plasmon resonances of multiple flat noble-metal nanostrips with a median-line integral equation technique," *IEEE Trans. Nanotechnol.*, vol. 12, no. 3, pp. 442–448, May 2013.
- [26] O. V. Shapoval and A. I. Nosich, "Finite gratings of many thin silver nanostrips: Optical resonances and role of periodicity," *AIP Adv.*, vol. 3, no. 4, 2013, Art. no. 042120.
- [27] O. Shapoval, A. I. Nosich, and J. Ctyroky, "Resonance effects in the optical antennas shaped as finite comb-like gratings of noble-metal nanostrips," *Proc. SPIE (Special Issue Integr. Opt.: Phys. Simul.)*, vol. 8781, 2013, Art. no. 87810U.
- [28] P. B. Johnson and R. W. Christy, "Optical constants of the noble metals," *Phys. Rev. B*, vol. 6, pp. 4370–4378, 1972.
- [29] A. Vial, T. Laroche, M. Dridi, and L. Le Cunff, "A new model of dispersion for metals leading to a more accurate modeling of plasmonic structures using the FDTD method," *Appl. Phys. A*, vol. 103, pp. 849–853, 2011.
- [30] A. Karlsson, "Approximate boundary conditions for thin structures," *IEEE Trans. Antennas Propag.*, vol. 57, no. 1, pp. 144–148, Jan. 2009.



**Olga V. Shapoval** (S'10–M'15) was born in Nikopol, Ukraine, in 1987. She received the M.S. (Hons.) degree in applied mathematics from Kharkiv National University, Kharkiv, Ukraine, in 2009, and the Ph.D. degree in radio physics from the Institute of Radio-Physics and Electronics, National Academy of Sciences of Ukraine (IRE NASU), Kharkiv, in 2014. She is currently a Senior Scientist with the Laboratory of Micro and Nano Optics, IRE NASU. Her research interests include computational electromagnetics, nanoscale optics and plasmonics, and modeling of lasers and sensors. She received the International Union for Radio Science Young Scientist Award for attending the Asia-Pacific Radio Science Conference in Toyama and the Doctoral Research Award from the IEEE Antennas and Propagation Society, both in 2010. In 2012, she received the Ph.D. Scholarship from the International Visegrad Fund. She also received the URSI Young Scientist Award for attending the Electromagnetic Theory Symposium in Hiroshima (2013), the Young Scientist Grant from the TICRA Foundation, Denmark (2014), and the Canon Foundation in Europe Research Fellowship (2016).



**Kazuya Kobayashi** (S'77–M'83–SM'99) received the B.S., M.S., and Ph.D. degrees in electrical engineering from Waseda University, Tokyo, Japan in 1977, 1979, and 1982, respectively. In 1982, he joined the Department of Electrical, Electronic, and Communication Engineering, Chuo University, Tokyo, Japan, where he is currently a Professor. Since 1987, he has held visiting professor positions at various institutions in Australia, China, Ukraine, and USA. His research interests include developments of rigorous methods as applied to electromagnetic wave

problems, radar cross-sectional manipulation, and canonical problems in wave scattering and diffraction. He is a member of the Science Council of Japan and a Fellow of the Electromagnetics Academy, and has held various URSI positions including President of the Japan National Committee of URSI (since 2008) and Vice-Chair of URSI Commission B (since 2014). He was involved in organizing a number of major international conferences including, AP-RASC, AT-RASC, EMTS, and PIERS.



**Alexander I. Nosich** (M'94–SM'95–F'04) was born in Kharkiv, Ukraine, in 1953. He received the M.S., Ph.D., and D.Sc. degrees in radio physics from Kharkiv National University, Kharkiv, Ukraine, in 1975, 1979, and 1990, respectively. Since 1979, he has been with the Institute of Radio Physics and Electronics, National Academy of Science of Ukraine, Kharkiv, where he is currently a Professor and Principal Scientist heading the Laboratory of Micro and Nano Optics. Since 1992, he has held a number of guest fellowship and professorship in the EU, Japan,

Singapore, and Turkey. In 2015, he was awarded the title of Docteur Honoris Causa of Université de Rennes 1, France. His research interests include the method of analytical regularization, propagation and scattering of waves, open resonators and open waveguides, simulation of micro- and nanocavity lasers, sensors, and antennas. He was one of the initiators and Technical Committee Chairman of the International Conference Series on Mathematical Methods in Electromagnetic Theory in 1989.